Quantitative studies on the microstructure of ternary CaO–Al2O3–SiO2 glasses by Raman spectroscopy, 27Al MAS NMR and quantum chemistry ab initio calculation

Xiaohui Tang, Jinglin You, Jian Wang, Fu Zhang, Xiaoye Gong, Yingfang Xie, Aurélien Canizarès, Catherine Bessada, Kai Tang, Liming Lu

Quantitative studies on the microstructure of ternary CaO-Al_2O_3-SiO_2 glasses by Raman spectroscopy, ^{27}Al MAS NMR and quantum chemistry *ab initio* calculation

Xiaohui Tang[a], Jinglin You[a, *], Jian Wang[a], Fu Zhang[a], Xiaoye Gong[a], Yingfang Xie[a], Aurélien Canizarès[b], Catherine Bessada[b], Franck Fayon[b], Kai Tang[c], Liming Lu[d]

[a] State Key Laboratory of Advanced Special Steel & Shanghai Key Laboratory of Advanced Ferrometallurgy & School of Materials Science and Engineering, Shanghai University, Shanghai, 200444, China
[b] CNRS, CEMHTI UPR3079, Université d'Orléans, Orléans, France
[c] SINTEF Industry, Trondheim, 7094, Norway
[d] Queensland Centre for Advanced Technologies, Technology Court, CSIRO Mineral Resources, Pullenvale, Queensland, 4069, Australia

Abstract: In order to investigate the structural behaviors of Al^{3+} in aluminosilicate system, the microstructural characteristics of CaO-SiO_2-based glassy samples with various Al_2O_3 contents were examined quantitatively by Raman spectroscopy and ^{27}Al MAS NMR. Sequence of multiple cluster models of aluminosilicate system modified with Ca^{2+} and Na^{+} cations have been designed, and Raman spectral simulation were carried out after geometric optimization by quantum chemistry (QC) *ab initio* calculation. The functional relationship between Raman scattering cross section (*RSCS*) and stress index of silicon-oxygen tetrahedron (*SIT*) for aluminosilicates was established, which was applied to the calibration of experimental Raman spectra successfully. Some five-fold coordinated aluminum (Al^{V}, around 5%) and less than 2% six-fold coordinated aluminum (Al^{VI}) were detected by ^{27}Al MAS NMR, while most of aluminum remained in tetrahedral sites (Al^{IV}). The ever-finer quantitative results of Raman spectroscopy and NMR showed a gradually production of Al^{IV} with the addition of Al_2O_3, along with the significant adjustment of Q_i species distribution, in which Q_1, Q_2 decreased and fully polymerized Q_4 increased while Q_3 showed a non-monotonic variation and obtained the maximum at Al_2O_3=18 mole%. Furthermore, the effects of aluminum to bridging oxygen bond types (T-O_b, T=Si, Al) and the degree of polymerization were also discussed in detail. These structural features related to composition are essential theoretic foundation to understand their properties.

Keywords: Calcium aluminosilicate glasses, Raman spectroscopy, ^{27}Al MAS NMR, Quantum chemistry *ab initio* calculation, Quantitative study

[*] Corresponding author.
E-mail addresses: jlyou@staff.shu.edu.cn (J. You).

1. Introduction

Among silicate systems, $CaO\text{-}Al_2O_3\text{-}SiO_2$ (CAS) glasses and melts are of special interest for their technological significance and structural peculiarities, and have a wide range of industrial applications [1-3]. For instance, CAS system is major compositions of blast furnace (BF) slags and mold fluxes extensively used in metallurgical process [4]. It is well known that the macroscopic physical and chemical properties of glass and melt are determined mainly by its microstructure, which have a strong dependence on its chemical composition. It is therefore essential to clarify the structure-composition relationship, before further understanding its properties.

In the ternary CAS system, the network former SiO_2 constructs various structural units through diverse connections of silicon-oxygen tetrahedrons (SiOTs), such as monomer (SiO_4), dimer (Si_2O_7), chain (SiO_3), layered (Si_2O_5) and three-dimensional network structure (SiO_2). These structural units also can be indicated by primary structural species Q_i (i=0-4, denotes the number of bridging oxygen (BO, O_b) in each tetrahedron) [5]. Moreover, You *et al*. [6] considered that the primary structure species are not enough to describe the complex connections among SiOTs, which need to employ hyperfine secondary structures adopted the shorthand symbol $Q^{jklm}_{i\,(n_1h,\,n_2q,\,n_3t)}$, where subscript *i* refers to the number of BO of the central SiOT; superscript *j*, *k*, *l* and *m* correspond to the numbers of BO of the adjacent tetrahedra Q_j, Q_k, Q_l and Q_m of the central Q_i, respectively; n_1, n_2 and n_3 are the number of various rings involved in the central SiOT, respectively, while *h*, *q* and *t* represent six, four and three membered rings, respectively .

Aluminum can play different roles in aluminosilicate glass because of its amphoterism. Four coordinated aluminum-oxygen tetrahedron (AlOT) exists commonly as the network former, which is corner-sharing with SiOT through BO, forming aluminosilicate frameworks. Unlike SiOT, however, owing to the requirement of charge balance, AlOT needs to consume alkali metal or alkaline-earth metal cations for charge compensation. Previous reports indicated that Ca^{2+} cation in calcium aluminosilicate is preferentially used to balance the charge of AlOT rather than as the network modifier to depolymerize the aluminosilicate network structure by providing non-bridging oxygen (NBO, O_{nb}) [4, 7]. In addition, aluminum may be found in five- and/or six-fold coordinated states in aluminosilicate, but their unambiguous structural features and formation mechanisms still remain unclear [8]. The effects of aluminum mainly depends on the ratio of CaO/Al_2O_3, i.e., whether there are sufficient metal cations for charge compensation [9, 10]. Moreover, it varies according to the properties and content of glass components and even glass formation conditions [11-14].

With the change of Al_2O_3 content, the structure of aluminosilicate will inevitably be greatly complicated, leading to changes in macroscopic physical and chemical properties. [15-20]. For instance, Wang *et al*. [21] revealed that with the addition of Al_2O_3, the initial crystallization temperature was raised while the reduction of

incubation time, due to more AlOT units polymerize with SiOTs to facilitate transformation of the primary phase. The studies on density showed [18, 19] that the density tended to decrease after increasing with the increase of Al_2O_3 content while R(CaO/SiO_2) =1, 1.3, owing to the amphoteric effect of Al_2O_3 on structure. Youngjo Kang *et al*. [22] reported the relationship between thermal conductivity and Al_2O_3 content with R(CaO/SiO_2) =0.39, 0.9, while the thermal conductivity exhibited maximum values when the mass of Al_2O_3 equaled from 15% to 20%. Overall, an in-depth understanding of the evolution of the aluminosilicate structure with the addition of alumina is crucial for determining property.

There are some spectroscopical techniques to extract structure details of amorphous silicate glasses. Among of them, Raman spectroscopy is one of the prevalent methods to investigate microstructures of vitrified and molten aluminosilicates. Some significant progresses have been achieved in the relationships among compositions, microstructures and properties of aluminosilicate [23-26]. In the Raman spectra of aluminosilicate, the characteristic Raman-active band in high wavenumber range (**>** 800 cm^{-1}) can be assigned to the symmetric stretching vibration of NBO of SiOT (Si-O_{nb}) which is approximately monotonically related to the type of central SiOT, that is, delicate $Q^{jklm}_{i\,(n_1h,\,n_2q,\,n_3t)}$ or primary Q_i species with different connections between central SiOT and adjacent tetrahedra, and is the object of Raman spectra quantification. Nonetheless, the quantitative analysis by Raman spectroscopy is still in dispute, one of which is the application of Raman scattering cross section (*RSCS*). Earlier quantitative studies by Raman spectroscopy directly evaluated the proportions of microstructures through the areas of multiple peaks obtained by deconvolution without considering the disturbing of *RSCS*. Actually, the intensities and areas of Raman spectral peaks are not linearly related to the contents of Q_i, because of the different polarizabilities. In recent years, scholars have paid more attention to the influence of *RSCS* while quantitatively analyzing Raman spectra [23-32]. Mysen *et al*. [25, 26] defined the relative sensitivity factor of various species Q_i, similar to the *RSCS*. You *et al*. [6, 31] proposed the concept of stress index of silicon-oxygen tetrahedron (*SIT*) to reflect the complex connectivities among SiOTs, in order to establish the relationship between *RSCS* and *SIT*, further quantitatively analyze the microstructures of binary sodium silicate. What's more, binary $CaO\text{-}SiO_2$ and ternary $MgO\text{-}CaO\text{-}SiO_2$ ternary system have been studied by MAS NMR and Raman spectroscopy along with quantum chemistry (QC) *ab initio* calculations method [27, 33]. Raman spectra has been corrected through the relationship among *SIT*, *RSCS* and vibration wavenumber, and the reliably quantitative analysis of Raman spectra was realized agreed well with NMR results.

Therefore, in the present work, *SIT* and *RSCS* values were employed to assist in quantitative investigating the evolutions of delicate $Q^{jklm}_{i\,(n_1h,\,n_2q,\,n_3t)}$ and primary Q_i species by Raman spectroscopy and simulation of calcium aluminosilicate glasses with various Al_2O_3 contents keeping a fixed CaO/SiO_2 ratio of 1. Additionally, the

roles of aluminum were also verified by ^{27}Al MAS NMR to thoroughly verify the effect of aluminum on the microstructure of aluminosilicate.

2. Experimental methods

2.1. Material synthesis

Six calcium aluminosilicate glassy samples were prepared by melting mixtures of CaO, Al_2O_3 and SiO_2. The compositions ranged from 0 to 30 mole percentage of Al_2O_3 at a constant CaO/SiO_2 ratio of 1, the sample compositions are shown in Table 1. After weighing, the starting materials with stoichiometric amounts of CaO, Al_2O_3 and SiO_2 (analytical reagent-grade, Sinopharm Chemical Reagent Co., Ltd) were mixed in an agate mortar for two hours with alcohol. The mixtures were then pressed into thin sheets with a diameter of 10 mm and a height of 1mm. An aerodynamic levitation (ADL) furnace, that was equipped with two beams of CO_2 lasers about 80 W and capable of achieving an extremely high cooling rate of 300 K/s, was applied for the preparation of glassy samples. The shorthand notation of CASx (x=0, 6, 12, 18, 24, 30) was adopted for the glassy samples with compositions of $(100-x)/2CaO \cdot xAl_2O_3 \cdot (100-x)/2SiO_2$.

Table 1 Chemical compositions of calcium aluminosilicate glassy samples.

Sample number	CaO/mol%	Al_2O_3/mol%	SiO_2/mol%
CAS0	50	0	50
CAS6	47	6	47
CAS12	44	12	44
CAS18	41	18	41
CAS24	38	24	38
CAS30	35	30	35

2.2. Experimental details

Raman spectra of calcium aluminosilicate glass samples from 50 to 1400 cm^{-1} were measured on Jobin Y'von LabRAM HR Evolution laser confocal Raman spectrometer, which equipped with an intensified charge coupled device (ICCD) detector. A visible pulsed laser beam of 532 nm was chosen to obtain excitation light, with the integration time and times of 10 and 30, respectively. The ×4 objective lens was applied to focus the laser beam on the glassy samples.

^{27}Al MAS NMR spectra of glassy samples were collected using Bruker Advance III WB 400 MHz spectrometer at Larmor frequency of 104.25 MHz (9.4 T). The samples were spun in cylindrical aluminum free zirconia rotors with 4 mm diameter at a spinning rate of 12 kHz. One-pulse acquisition was used while the cycle delay time was 0.5 s, and the cumulative times were 600.

2.3. Computational details

The cluster models of ternary CaO-Al_2O_3-SiO_2 aluminosilicate with different aluminum introduction and various Q_i connections were constructed on the basis of CaO-SiO_2 binary silicates, which were optimized and calculated by QC *ab initio* calculations by using Gaussian 09W software. The Restricted Hartree-Fock (RHF) self-consistent field and 6-31G(d) basis set were employed to optimize clusters and Raman spectra were then simulated for those clusters after being optimized on the same computational methodology [34, 35].

It is worth noting that the 'Loewenstein Al avoidance' rule [36] was preferentially considered for the introduction position and amount of Al of cluster models construction. In consideration of charge balance of AlOTs, a cluster structure with n(Al) requires 1/2n(Ca) as the role of charge compensation, which greatly increased the difficulty of cluster structure construction to maintain higher symmetry and reduced the computational success. Therefore, Na^+ cation was selected to partially displace Ca^{2+} cation as charge compensated ion in order to simulate more reliable structures. Previous studies showed that the influence of different alkali metal and alkaline earth metal cations on the symmetric stretching vibration frequency of $Si\text{-}O_{nb}$ in silica tetrahedral structure units can be negligible [37, 38].

3. Results and discussion

3.1. QC *ab initio* calculations of cluster models

About the description of Q_i species distribution of SiOT units in silicate and aluminosilicate glasses, great efforts have been made for several decades [39-42]. Recently, the accurate ^{29}Si NMR results for binary silicate glasses have showed that five Q_i species with the value of i varies from 0 to 4 were regularly distributed, which characterize the complicated network connectivity and chemical local order, mainly depending on content, composition and formation conditions, *etc*. [6, 27, 42-45]. You and Ma *et al*. [6, 27] concretized Q_i species in alkali and alkaline earth silicate glasses/melts into multimolecular clusters to simulate the connections of Q_i, in which SiOTs are interconnected with each other to form chain, ring and framework structures, while cations are evenly located around the NBOs as network modifiers for charge compensation. In this work, a series of cluster models were designed with connections of AlOTs and SiOTs as network formers while Ca^{2+} cations acted as network modifiers, and Na^+ cations were used while being necessary to balance the charge of AlOTs.

The optimized cluster models by QC *ab initio* calculations with different connections have been illustrated in Fig. 1. The calculated Raman-active wavenumber of symmetric stretching vibrations of $Si\text{-}O_{nb}$ and its *RSCS* are shown in Table 2. The calculation results indicate that the characteristic peaks with notable intensity in 800-1200 cm^{-1} are mainly the symmetric stretching vibrations of $Si\text{-}O_{nb}$. The

wavenumbers of identical Q_i species in this range decreased with the increase of aluminum introduction, which is well consistent with the results of kyanite, sillimanite and andalusite by Pan *et.al* [46]. It can be attributed to that, comparing to Si-O bond, Al-O bond has smaller force constant, and the coupling of Al-O and Si-O bond leads to the decrease of wavenumber of Si-O_{nb} symmetrical stretching vibration. Brawer and White [38] pointed out that the variation of Raman shifts of Si-O_{nb} bond in ternary aluminosilicates such as Na_2O-Al_2O_3-SiO_2 attributed to the substitution of Al^{3+} for Si^{4+} and changed the morphology of microstructures. Therefore, symmetric stretching vibration of Si-O_{nb} bonds sensitively reflect the change of aluminosilicate microstructures, and is the significant subject for the study of aluminosilicate microstructures by Raman spectroscopy.

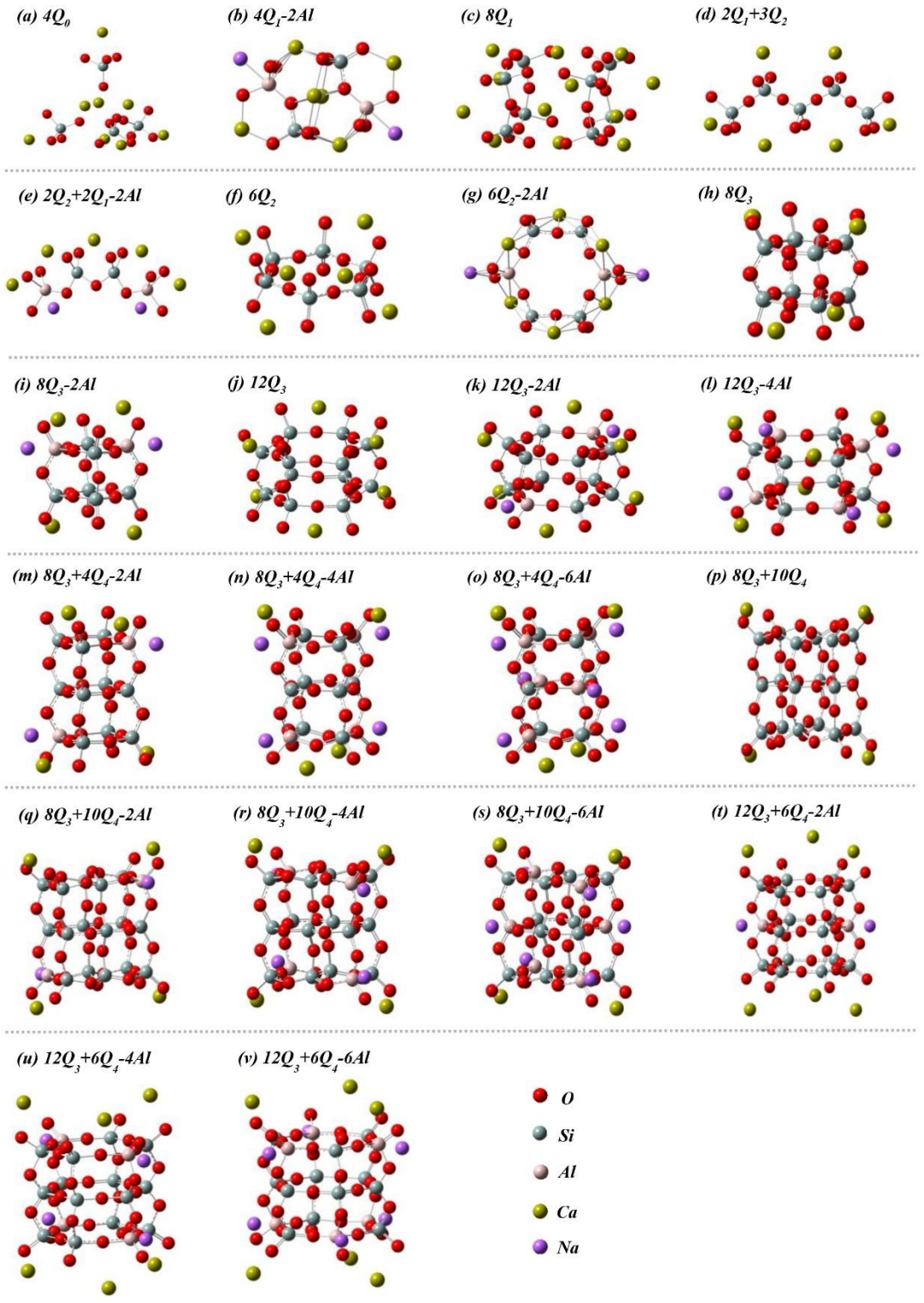

Fig. 1. Diagrams of cluster models with different connection between central silicon-oxygen tetrahedron (SiOT) and adjacent SiOT or aluminum-oxygen tetrahedra (AlOT), forming network framework. Meanwhile Ca^{2+} cations act as network modifiers, and Na^{+} cations act as charge compensators of AlOTs, partially replace Ca^{2+} : (a) $Ca_8Si_4O_{16}$; (b) $Ca_6Si_4O_{14}$; (c) $Ca_6Na_2Si_2Al_2O_{14}$; (d) $Ca_6Si_5O_{16}$; (e) $Ca_5Si_4O_{13}$; (f) $Ca_6Si_6O_{18}$; (g) $Ca_6Na_2Si_4Al_2O_{18}$; (h) $Ca_4Si_8O_{20}$; (i) $Ca_4Na_2Si_6Al_2O_{20}$; (j) $Ca_6Si_{12}O_{30}$;

(k) $Ca_6Na_2Si_{10}Al_2O_{30}$; (l) $Ca_6Na_4Si_8Al_4O_{30}$; (m) $Ca_4Na_2Si_{10}Al_2O_{28}$; (n) $Ca_4Na_4Si_8Al_4O_{28}$; (o) $Ca_4Na_4Si_6Al_6O_{28}$; (p) $Ca_6Na_2Si_{16}Al_2O_{42}$; (q) $Ca_6Na_4Si_{14}Al_4O_{42}$; (r) $Ca_6Na_6Si_{12}Al_6O_{42}$; (s) $Ca_4Si_{18}O_{40}$; (t) $Ca_4Na_2Si_{16}Al_2O_{40}$; (u) $Ca_4Na_4Si_{14}Al_4O_{40}$; (v) $Ca_4Na_4Si_{14}Al_4O_{40}$.

The wavenumbers of Si-O_{nb} symmetric stretching vibration in Raman spectra predominantly reflect the types of delicate $Q^{jklm}_{i\,(n_1h,\,n_2q,\,n_3t)}$ or primary Q_i species, which actually reveal the local microscopic environment of the interior stress of SiOT. Consequently, in order to explain the microscopic stress functioning mechanism and establish the relationship between wavenumbers and microstructures, the *SIT* of SiOT was empirically defined by You. *et al* [6]. In previous studies on silicates, the linear relationship between *SIT* and wavenumbers of Si-O_{nb} symmetric stretching vibration has been obtained, and *SIT* has been applied effectively in qualitative analysis of the microstructures by Raman spectroscopy [6, 27, 31]. As mentioned above, introduction of aluminum will heavily affect the symmetrical stretching vibration of Si-O_{nb}. Therefore, in order to establish the relationship between microstructural stress and characteristic Raman vibration wavenumbers in ternary CaO-Al_2O_3-SiO_2 system, the influence of aluminum on microscopic stress environment is necessary to be considered. The developing calculation formula of *SIT* as follows:

$$SIT = {}^1X_i + \alpha R \qquad (1\text{-}1)$$

$${}^1X_i = \frac{1}{i}\left(\sum_{j=1}^{k}\sqrt{Q_iQ_{(j)}} + \beta\sum_{j=k+1}^{i}\sqrt{Q_iQ_{(j)}}\right) \qquad (1\text{-}2)$$

$$R = \sum_1^m \frac{n_{Si}+\beta n_{Al}}{n_i(n_i-2)} \qquad (1\text{-}3)$$

Where ${}^1X_i$ is the first-order molecular connectivity index of SiOT, while R and α are the contribution of the ring and the proportionality coefficient (α=1 in non-alumina silicate), respectively [6]. Q_i is the number of BO in the *i*th SiOT, while Q_j is the BO number of SiOT or AlOT adjacent to the *i*th SiOT. The parameter of n_i is the number of rings Q_i participating in while n_{Si} and n_{Al} are the number of rings SiOT and AlOT participating in, respectively. β is a constant, which represents the stress effect of an AlOT on its nearest SiOT. After fitting optimization, the relationship between fitting coefficient R^2 and β showed that when β=0.5, the calculated wavenumber of Si-O_{nb} symmetric stretching vibration mode displays a best linear correlation with the corresponding *SIT* value [47]. The values of *SIT* in the clusters are presented in Table 2.

Table 2 The number of aluminum introduction, stress index of silicon-oxygen tetrahedron (SIT), Raman scattering cross section (RSCS), and the wavenumber of symmetric stretching vibration of Si-O_{nb} by quantum chemistry ab initio calculation of designed cluster models probably existed in ternary CaO-Al_2O_3-SiO_2 glasses.

Chemical formula	Q_i species	Al number	*SIT*	*RSCS*	Si-O_{nb} stretching/cm^{-1}

(a) $Ca_8Si_4O_{16}$	$4Q_0$	0	0	11.39	902
(b) $Ca_6Si_4O_{14}$	$4Q_1$	0	1	5.87	949
(c) $Ca_6Na_2Si_2Al_2O_{14}$	$2Q_1$	2	0.5	9.29	936
(d) $Ca_6Si_5O_{16}$	$2Q_1+3Q_2$	0	1.71	5.46	1013
(e) $Ca_5Si_4O_{13}$	$2Q_1+2Q_2$	2	1.35	7.58	993
(f) $Ca_6Si_6O_{18}$	$6Q_2$	0	2.25	5.4	1024
(g) $Ca_6Na_2Si_4Al_2O_{18}$	$6Q_2$	2	1.708	6.2	983
(h) $Ca_4Si_8O_{20}$	$8Q_3$	0	4.5	3.47	1149
(i) $Ca_4Na_2Si_6Al_2O_{20}$	$8Q_3$	2	3.875	1.56	1099
(j) $Ca_6Si_{12}O_{30}$	$12Q_3$	0	4.25	3.29	1142
(k) $Ca_6Na_2Si_{10}Al_2O_{30}$	$12Q_3$	2	3.854	1.56	1105
(l) $Ca_6Na_4Si_8Al_4O_{30}$	$12Q_3$	4	3.302	2.15	1068
(m) $Ca_4Na_2Si_{10}Al_2O_{28}$	$8Q_3+4Q_4$	2	4.218	2.95	1127
(n) $Ca_4Na_4Si_8Al_4O_{28}$	$8Q_3+4Q_4$	4	3.405	2.71	1071
(o) $Ca_4Na_4Si_6Al_6O_{28}$	$8Q_3+4Q_4$	6	2.702	4.24	1021
(p) $Ca_6Na_2Si_{16}Al_2O_{42}$	$12Q_3+6Q_4$	2	4.129	2.34	1147
(q) $Ca_6Na_4Si_{14}Al_4O_{42}$	$12Q_3+6Q_4$	4	3.801	1.65	1101
(r) $Ca_6Na_6Si_{12}Al_6O_{42}$	$12Q_3+6Q_4$	6	3.218	2.07	1064
(s) $Ca_4Si_{18}O_{40}$	$8Q_3+10Q_4$	0	4.809	4.05	1173
(t) $Ca_4Na_2Si_{16}Al_2O_{40}$	$8Q_3+10Q_4$	2	4.6	3.33	1154
(u) $Ca_4Na_4Si_{14}Al_4O_{40}$	$8Q_3+10Q_4$	4	4.184	3.01	1131
(v) $Ca_4Na_4Si_{14}Al_4O_{40}$	$8Q_3+10Q_4$	6	3.482	1.4	1108

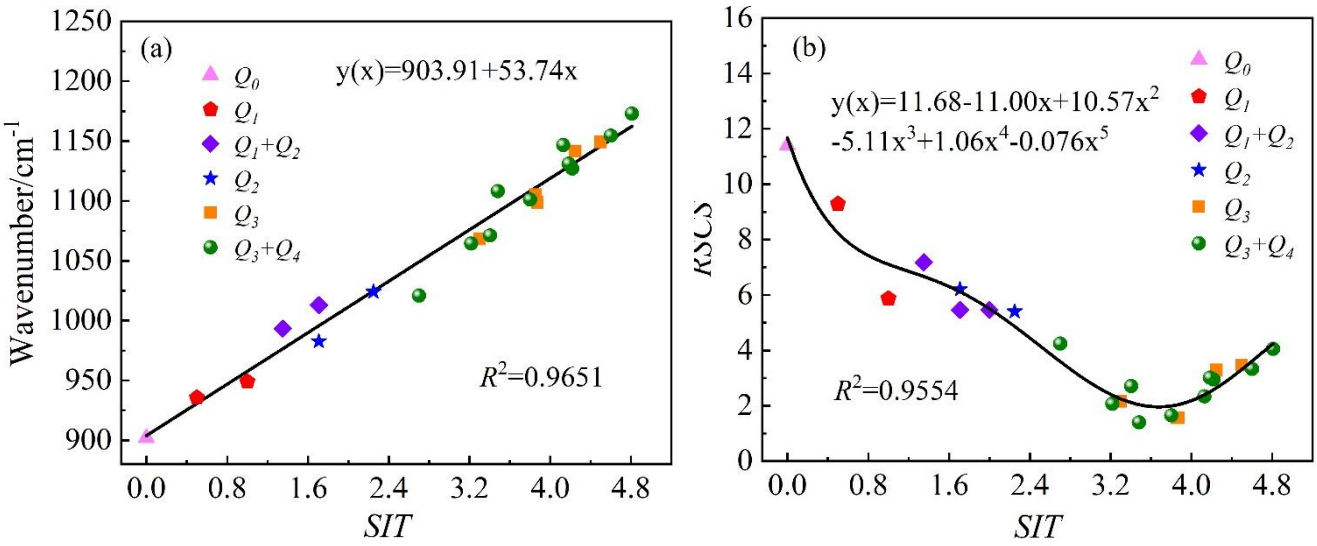

Fig. 2. (a) Fitted linear relationship between stress index of silicon-oxygen tetrahedron (SIT) and Wavenumber of Si-O_{nb} symmetric stretching vibration and (b) Fitted relationship between SIT and Raman scattering cross section (RSCS) by polynomial regression, where the icons with different shapes and colors refer to the original fitting data (i.e., the calculated Q_i by quantum chemistry ab initio calculation based on the designed probable cluster microstructures in calcium aluminosilicate).

The linear relationship between the *SIT* of Q_i and the calculated wavenumber of Si-O_{nb} symmetric stretching vibration is established, as shown in Fig. 2 (a) which is well consistent with that of binary sodium silicates and calcium silicate in previous studies [6, 27]. The determination of this relationship is well proved that the concept of *SIT* can be extended to ternary calcium aluminosilicate glasses. On the other hand, theoretically, Q_i with different *SIT* has its specific *RSCS* value, and the relationship between *SIT* and *RSCS* shows in Fig. 2 (b) which was fitted by polynomial regression. This polynomial function will be applied to correct experimental Raman spectra of glasses, and then the relative concentrations of Q_i in calcium aluminosilicate glasses can be obtained from the areas of the corrected Raman spectra.

3.2. ^{27}Al MAS NMR spectra

As a powerful approach, ^{27}Al MAS NMR spectra can probe subtle variations of the local environment of aluminum effectively. Consequently, in order to identify the roles of aluminum in aluminosilicate network, ^{27}Al MAS NMR spectra of prepared glassy samples were obtained, as shown in Fig. 3.

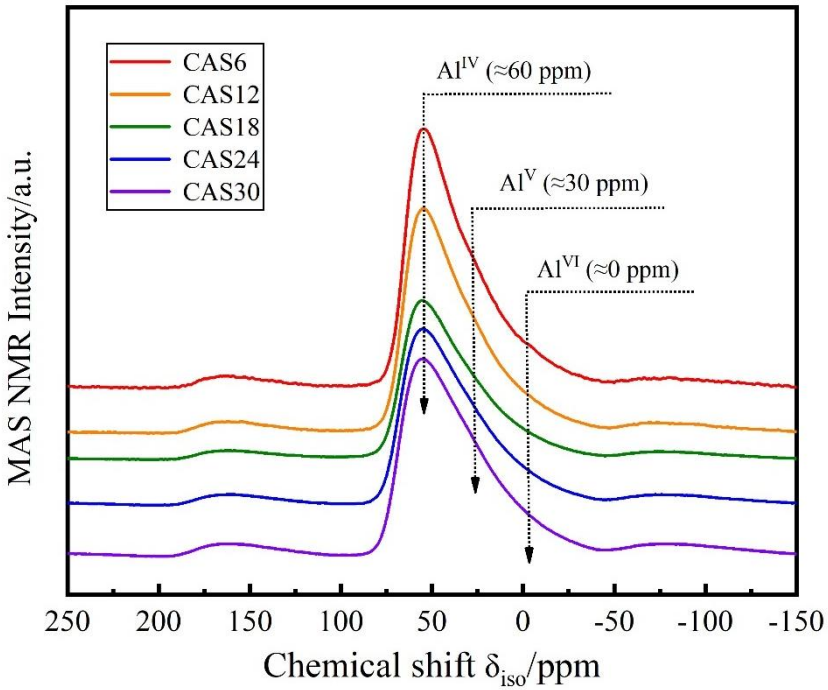

Fig. 3. Experimental ^{27}Al MAS NMR spectra of CAS6, CAS12, CAS18, CAS24, CAS30 glassy samples recorded at the magnetic field of 9.4T.

It displays a series of relatively broad peaks in all samples which is the feature of NMR spectrum of amorphous aluminosilicate due to dipolar interactions, anisotropy of the chemical shielding and quadrupolar interactions [48]. Concurrently, the ^{27}Al MAS NMR spectra for five glasses exhibit a dominant asymmetric peak (around 60 ppm) with a shoulder (around -20-40 ppm), which denote the chemical shift of Al^{IV}, Al^{V} and Al^{VI}, respectively. Significantly, the ^{27}Al MAS NMR spectra in this study were recorded at a relatively moderate magnetic field intensity of 9.4 T, resulting in a long intensity tail to lower frequency due to the strong second-order quadrupolar coupling effect of aluminum, because of the wide distribution of quadrupolar coupling constants (C_Q) at low field strength essentially [8, 49], which will cover and obscure the possible peaks of Al^{V} and Al^{VI}. S. Sukenaga *et al*. [50] reconsidered the coordination of aluminum in CAS glasses by using high field strength solid-state NMR spectroscopy. Compared with the results of ^{27}Al MAS NMR spectra obtained under low field strength (7.0 T), the influence of second-order quadrupolar broadening under higher field strength (16.4 T) is significantly reduced while chemical shift distribution effects are enhanced and the masked Al^{V} small shoulder can also be distinguished. In addition, it can be observed that the NMR spectra show almost the undifferentiated chemical shift and subtle change of full width at half maximum (FWHM). This phenomenon implies that the local environments of aluminum with different constituent have not changed significantly, i.e., the presence of aluminum in fourfold coordination predominantly acting as network former.

To consider the effect of second-order quadrupolar interaction, the spectra were fitted in DMFit [51] software by using Czjzek line shapes, which allows fitting of the

experimental spectra with average isotropic chemical shift value (δ_{iso}), distribution, and mean C_Q, to simulate the second-order quadrupolar broadened peaks from aluminum in different coordination environments. The fitting results of obtained ^{27}Al MAS NMR spectra are shown in Table 3, and the example of fitting spectrum is plotted in Fig. 4.

Table 3 The fitting parameters of relative intensity (I), average isotropic chemical shift (δ_{iso}), full width at half maximum of the Czjzek distribution (FWHM) and average quadrupolar coupling constant (C_Q) using Czjzek line shapes to the ^{27}Al MAS NMR spectra of glassy samples.

sample	Coordination environment	I/%	δ_{iso}/ppm	FWHM/ppm	C_Q/MHz
CAS6	Al^{IV}	93.41	65.45	12.86	6.26
	Al^{V}	5.15	33.20	12.76	5.54
	Al^{VI}	1.44	7.97	13.75	5.26
CAS12	Al^{IV}	93.80	66.62	13..36	6.50
	Al^{V}	4.60	35.17	14.39	5.41
	Al^{VI}	1.60	6.57	12.70	5.26
CAS18	Al^{IV}	97.19	67.83	13.89	6.74
	Al^{V}	2.81	34.57	14.39	5.55
	Al^{VI}	-	-	-	-
CAS24	Al^{IV}	96.98	68.76	13.86	7.08
	Al^{V}	3.02	37.84	14.39	5.55
	Al^{VI}	-	-	-	-
CAS30	Al^{IV}	93.11	65.58	12.26	6.33
	Al^{V}	5.25	34.16	14.39	5.73
	Al^{VI}	1.64	7.14	12.70	5.26

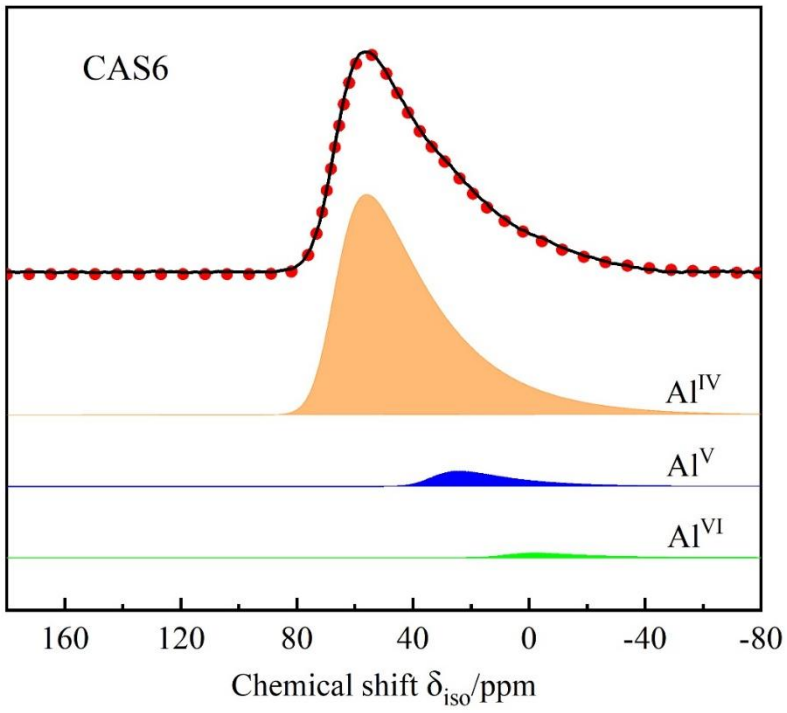

Fig. 4. The fitting result of ^{27}Al MAS NMR spectrum of CAS6 glassy sample using Czjzek line shapes, where black solid line is original spectrum, and red dotted line is the sum of Al^{IV}(orange area), Al^{V} (blue area), and Al^{VI}(green area).

For all investigated glasses, most of aluminum atoms are in fourfold coordinated Al^{IV} sites (more than 90%, Table 3). Furthermore, a substantial fraction of fivefold coordinated Al^{V} sites are detected (around 5%, Table 3) while the presence of a minor amount (less than 2%, Table 3) of sixfold coordinated Al^{VI} sites, as shown in Fig. 6. Theoretically, in peralkaline(-earth) field, aluminum atoms are stabilized in tetrahedral position without forming higher coordinated species due to have enough Ca^{2+} ions for charge compensation of AlOTs. However, previous studies on ^{27}Al MQ-MAS NMR confirmed that [9, 13, 49, 52, 53], less than 10% of high coordinated Al^{V} and Al^{VI} were observed even for percalcic CAS glasses. And this counter-intuitive conclusion is further borne out by ^{27}Al MAS NMR results of present samples. The mean values of C_Q were collected of different aluminum sites, which are in accord with typical C_Q values in the 5-10 MHz range [8].

The δ_{iso} values of three aluminum sites of five glassy samples have almost unchanged, as shown in Fig. 5. It verifies the extrapolation, that the local environment of Al^{IV} sites is settled as network formers, and further demonstrates that Al^{IV} atoms preferentially occupy fully polymerized Q_4 sites with δ_{iso} around 55-70 ppm [8] without NBO associated with, which has concluded through Raman and NMR results [26, 54]. Fig. 6 also exhibits the molar ratio of $Al^{IV}/(Al^{V}+Al^{VI})$ with differing Al_2O_3 contents, which increases with the increasing Al_2O_3 firstly, and then decreases in samples of CAS24 and CAS30 glasses. Although the amounts of Al^{V} and Al^{VI} are insignificant leading to the variation is likely caused by errors, it should not be neglected and be further studied by using higher resolution technology.

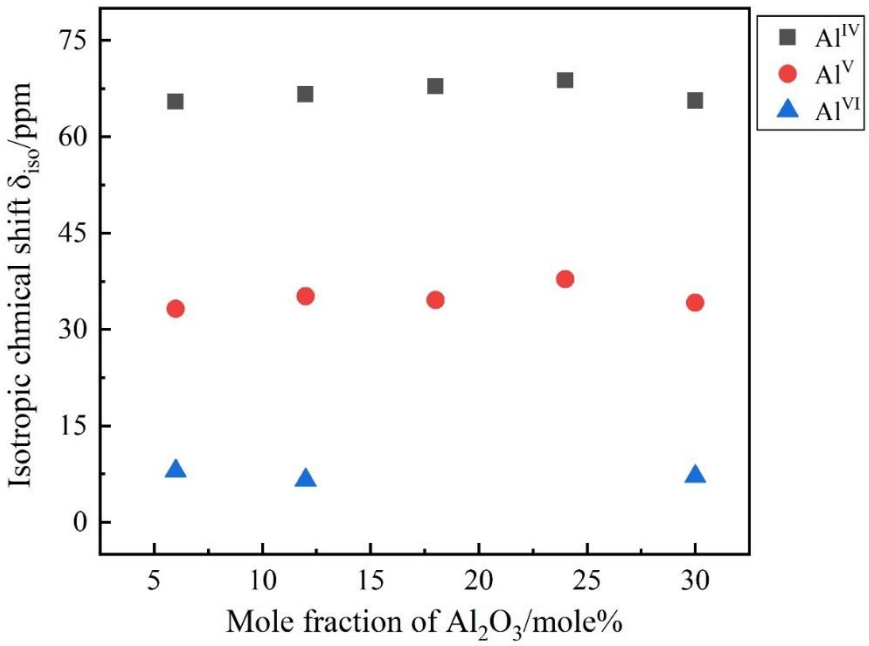

Fig. 5. Dependence of the isotropic chemical shifts (δ_{iso}) for Al^{IV}, Al^{V}, Al^{VI} species on Al_2O_3 contents.

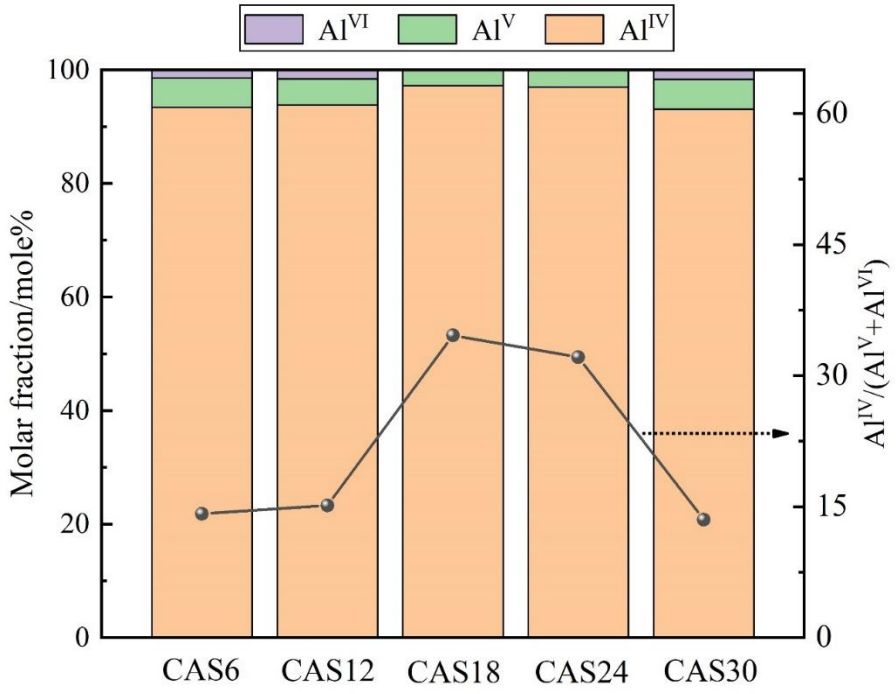

Fig. 6. The molar fractions of Al^{IV}, Al^{V}, Al^{VI} (corresponding to the column and left axis) and molar ratio of $Al^{IV}/(Al^{V}+Al^{VI})$ (corresponding to the curve and right axis) in calcium aluminosilicate glasses.

3.3. Raman spectra of calcium aluminosilicate glasses

3.3.1 Qualitative analysis of Raman spectra

Raman spectra of all components glassy samples are plotted in Fig. 7 (a). For alumina free CAS0 glass, it can be roughly distinguished into three regions. For low-frequency range between 200-400 cm^{-1}, in addition to the vibration caused by modifier cations (Ca-O), which can mainly be associated to the lattice vibrations of the skeleton or framework with a broad band centered near 350 cm^{-1}, reflecting the long-distance order of structure. Its relative intensity decreases significantly with the adding of Al_2O_3, until vanishes completely at $x \geq 18$, which indicates the disorder degree of silicate network increased violently, and the remained ordered region of glassy structure disappeared completely at $x \geq 18$. On the other hand, the similar phenomenon was detected by depolarized Raman spectra for ternary CAS system [55], which considered the band of 350 cm^{-1} originated from cations at modifier place and its intensity decreased much faster than the CaO concentration. As such, it also demonstrates that the role of calcium may change due to the appearance of AlOTs, and Ca^{2+} ions behave preferentially to balance the charge of AlOTs after adding Al_2O_3.

Intermediate frequency range of 400-800 cm^{-1} corresponds to the symmetric bending vibration of the Si-O_b-Si linkages in silicate. For the CAS0 glass, a strong band at 622 cm^{-1} is displayed, assigned to the bending vibrations of Si-O_b-Si linkages.

With the increase of Al_2O_3 content, the relative intensity decreases sharply and disappears at x＞18. Correspondingly, a new large band grows at 570 cm^{-1} with a shoulder near 508 cm^{-1}, which reflects the motions of bridging oxygen in T-O_b-T linkages (T=Si or Al) [9]. These features resemble those were observed in other aluminosilicate systems [9, 44, 53], which indicated similarly that aluminum partly substituted for silicon and participated in the formation of network.

For high-frequency range 800-1200 cm^{-1}, which is the most informative Raman characteristic band with the strongest relative intensity. Mysen *et al*. [56] testified that the band in this region belongs to the symmetric stretching vibration of Si-O_{nb}, which is the sum of various Q_i species centered on SiOTs with diverse connections, reflecting the significant microstructural characteristics of aluminosilicates.

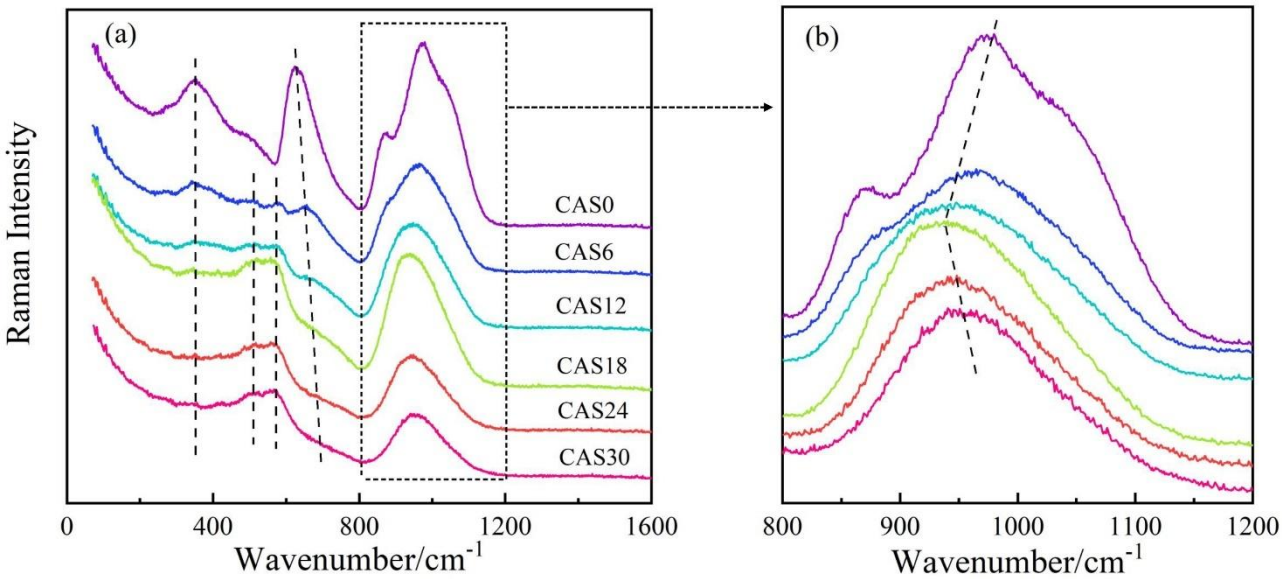

Fig. 7. (a) Raman spectra of CASx (x=0, 6, 12, 18, 24, 30) glasses; (b) Raman characteristic peaks in the region of 800-1200 cm^{-1}.

All glasses exhibit a distinct band in this range (as shown in Fig. 7 (b)), and as Al_2O_3 content increases, a decrease of wavenumber is observed at x＜18, while appearing the opposite trend at x≥18. Rajavaram *et al*. [19] acquired the analogous tendency, except the different turning point at x=15. They considered that it was the formation of AlOTs firstly at x＜15, owing to enough Ca^{2+} cations as charge compensation ions of AlOTs, which were consumed at x≥15, and Al^{V}, Al^{VI} units formed. However, this conclusion should be reconsidered, because CaO/Al_2O_3>1 is satisfied in all glassy samples, besides that, ^{27}Al MAS NMR fitting results show inconspicuous proportions of Al^{V} and Al^{VI}. Considering this wide envelope contains manifold unresolved delicate $Q^{jklm}_{i\,(n_1h,\,n_2q,\,n_3t)}$, it is essential to deconvolute the Raman spectra with different types of microstructure species and further investigate the characteristics of microstructure.

3.3.2 Quantitative analysis of Raman spectra

About the deconvolution of high-frequency range of 800-1200 cm^{-1}, it should be pointed out that the original experimental spectra must be calibrated, while applying the results of QC *ab initio* calculation in experimental quantitative analysis of the microstructure units of aluminosilicates, including the temperature correction by Bose-Einstein factor and frequency correction by the excitation sources [6, 27, 28, 33, 57]. Relative equation derived from the fundamental theory of Raman scattering for Stokes components was proposed to correlate the relative Raman intensities (I_i) [58, 59].

$$I_i = \frac{f(\nu_0-\nu_i)^4}{\nu_i\left(1-e^{-\frac{hc\nu_i}{kT}}\right)}S_i \qquad (2)$$

Where S_i is the calculated Raman activities, ν_0 is the exciting wavenumber of the laser source (in cm^{-1}); ν_i is the vibrational wavenumber of the *i*th normal mode; *f* is a suitably chosen common scaling factor for all the peak intensities; *h*, *c* and *k* are the Planck's constant, velocity of light and Boltzmann constant, respectively. What mentioned above, *RSCS* is a significant correction coefficient concatenates the ratio of Raman peak intensity and the concentration of microstructure species. Therefore, in order to obtain the microstructure contents of calcium aluminosilicates, Eq. (3) was used for frequency correction of the original Raman spectra.

$$I(x) = \frac{f(x)}{g(x)} \qquad (3)$$

Where *I(x)* is the corrected Raman intensity, while f(x) is the original Raman intensity, and *g(x)* is the functional relationship between *RSCS* and wavenumber, which was obtained by the consideration of both relationships between wavenumber-*SIT* (Fig. 2 (a)) and *RSCS*-*SIT* (Fig. 2 (b)).

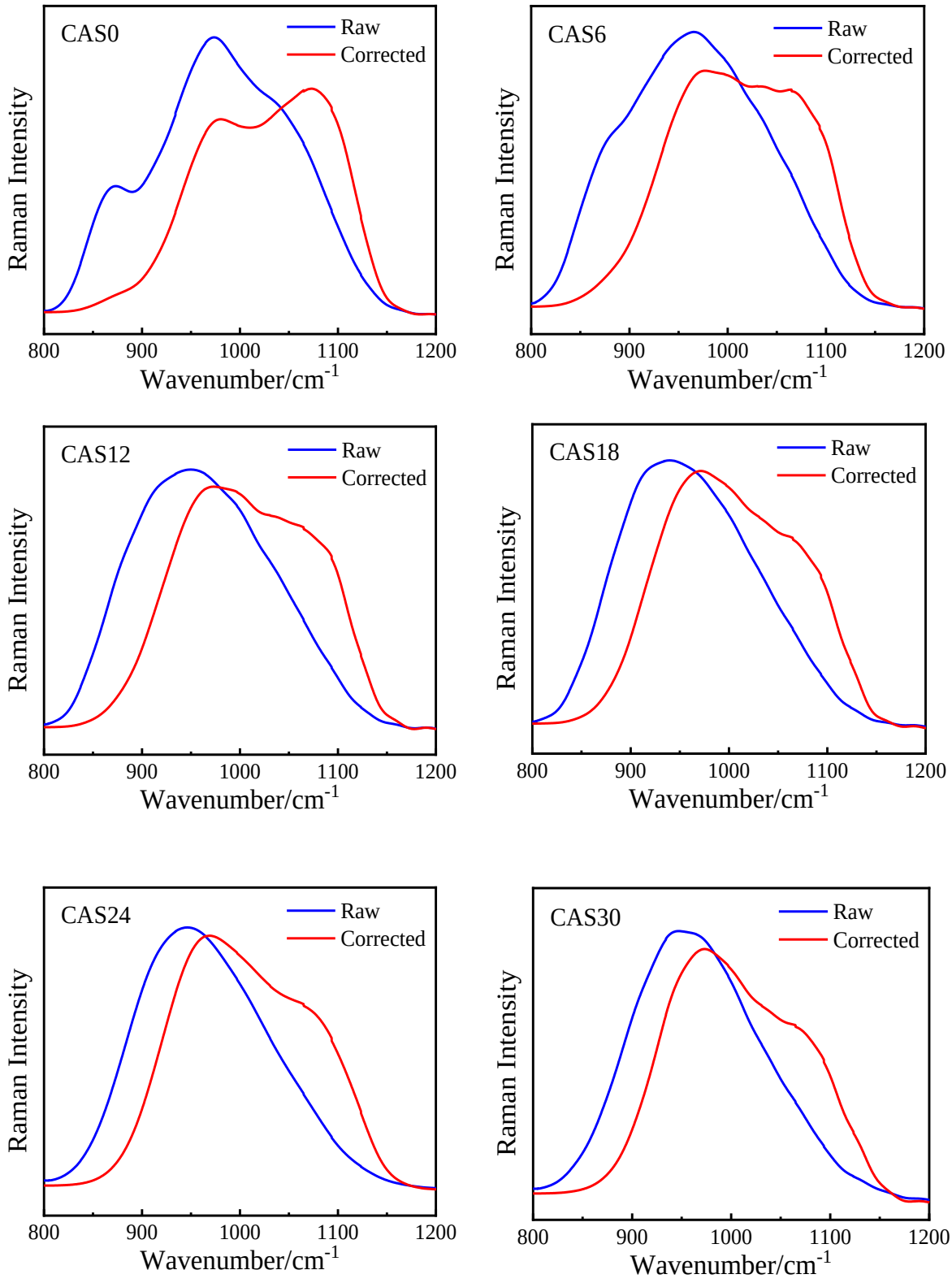

Fig. 8. Original Raman spectra of CASx (x=0, 6, 12, 18, 24, 30) glassy samples in the range of 800-1200 cm^{-1} and corresponding corrected Raman spectra by RSCS calibration process.

Fig. 8 shows the comparison between corrected and original Raman spectra, which a significant distinguish is uncovered both in shape and appearing peak positions. This is the results of $Q^{jklm}_{i\,(n_1h,\,n_2q,\,n_3t)}$ with different optical sensitivities, and the corrected curve can reflect the authentic $Q^{jklm}_{i\,(n_1h,\,n_2q,\,n_3t)}$ species contents. The correction and deconvolution of binary $CaO\text{-}SiO_2$ and $MgO\text{-}SiO_2$ glasses were carried out in the same way by researchers [27, 33], whose results were well consistent with the quantitative results of ^{29}Si MAS NMR, which verified the reliability of the correction curve and the accuracy of *RSCS* calculated by QC *ab initio* calculations. The delicate structures of glassy samples are obtained by deconvolution of the corrected Raman spectra, as illustrated by CAS6 sample in Fig. 9.

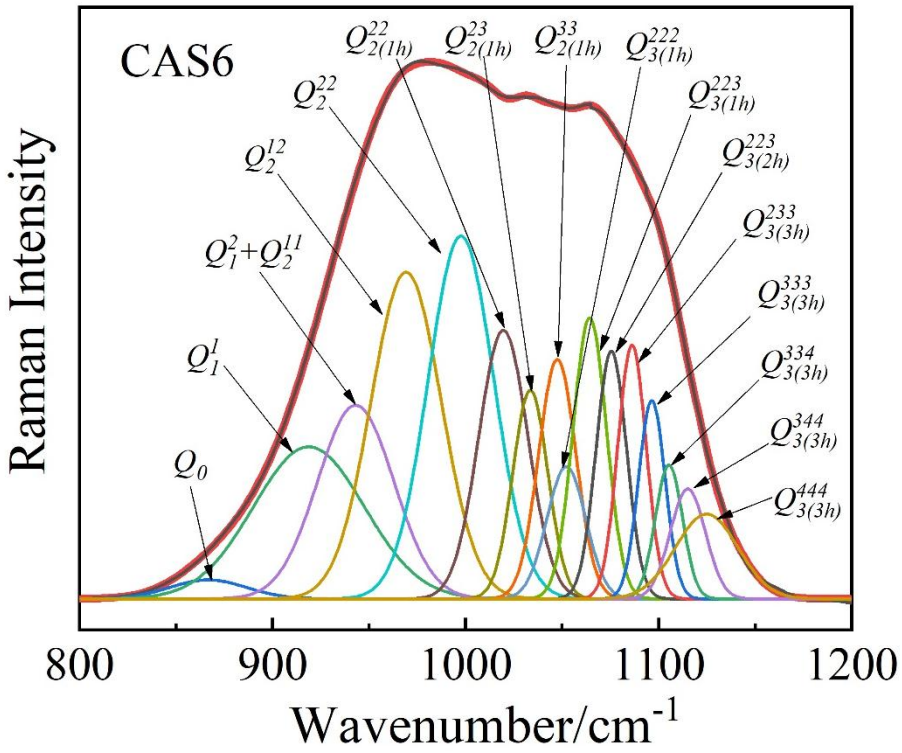

Fig. 9. Deconvolution of the corrected Raman spectrum of CAS6 glass sample by Gaussian function, where black solid line is original spectrum and red solid line is the sum of sixteen delicate structure peaks $Q^{jklm}_{i(n_1h,n_2q,n_3t)}$ *which reflect the different connections between central SiOT and adjacent tetrahedra.*

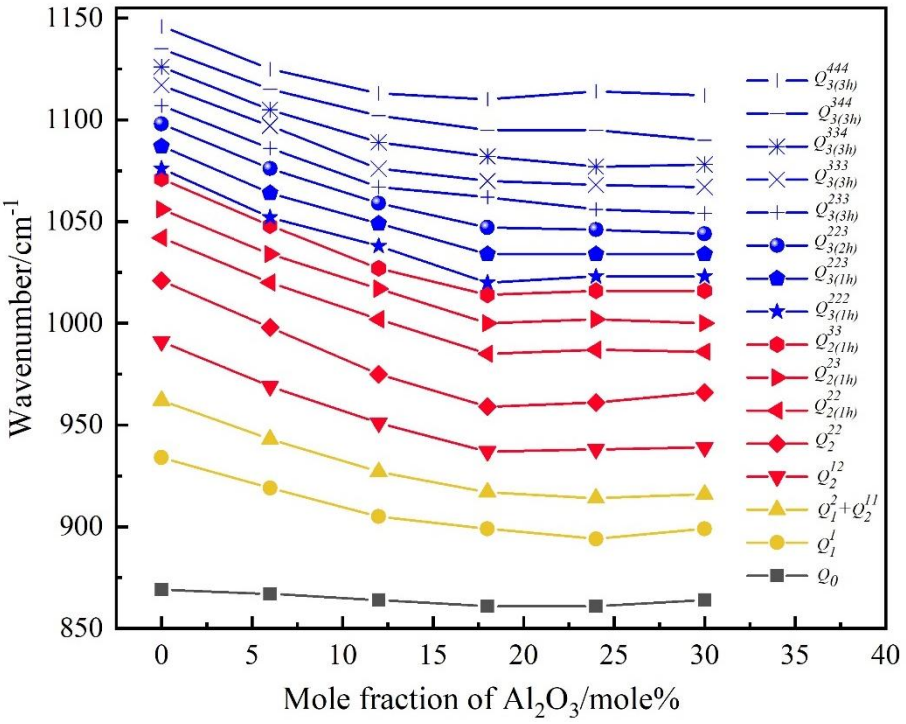

Fig. 10. The quantitative distribution of sixteen delicate structures $Q^{jklm}_{i\,(n_1h,\,n_2q,\,n_3t)}$ *centered on SiOTs with the addition of* Al_2O_3.

Previous studies have demonstrated that in silicates while the network former contains only silicon, the Si-O_{nb} vibrational wavenumbers of hyperfine structure $Q^{jklm}_{i\,(n_1h,\,n_2q,\,n_3t)}$ maintain constant with the change of composition [27]. Differentially, except Q_0, the wavenumbers of $Q^{jklm}_{i\,(n_1h,\,n_2q,\,n_3t)}$ change with the increase of Al_2O_3 contents, as shown in Fig. 10, while $Q^{jklm}_{i\,(n_1h,\,n_2q,\,n_3t)}$ has a red shift in $x<18$, but remains almost constant in $x\geq18$. It can be elucidated that, while four-fold coordinated aluminum enters the silicate structure as a network former, the coupling of Al^{IV}-O and Si-O causes the red shift of Si-O_{nb} symmetric stretching vibration. Meanwhile, the variation tendency indicates the coupling effect disappears when $x\geq18$.

After considering *RSCS*, the Gaussian deconvolution was carried out based on the delicate structures $Q^{jklm}_{i\,(n_1h,\,n_2q,\,n_3t)}$, and the peak areas of specific $Q^{jklm}_{i\,(n_1h,\,n_2q,\,n_3t)}$ is proportional to its abundance. Then $Q^{jklm}_{i\,(n_1h,\,n_2q,\,n_3t)}$ belonging to the same type of Q_i species can be summed to obtain the relative overall contents of each primary structure Q_0, Q_1, Q_2 and Q_3 respectively as shown in Fig. 11. It is manifest that except Q_0, Q_i (i=1, 2, 3) are asymmetric bands, which well confirms the results of Zhang *et al*. [60, 61] by ^{29}Si MAS NMR. Their research revealed the incomplete symmetry of spectra of various Q_i, in which Q_0 and Q_4 are completely symmetrical, and Q_1, Q_3 and

Q_2 asymmetry increase in turn. Therefore, it is significant to obtain the more precise results while applying the delicate structural deconvolution, rather than deconvoluting the symmetrical bands of primary structures Q_i directly which is insufficient for describing the real structure or the practical connectivity between central SiOT and adjacent tetrahedra.

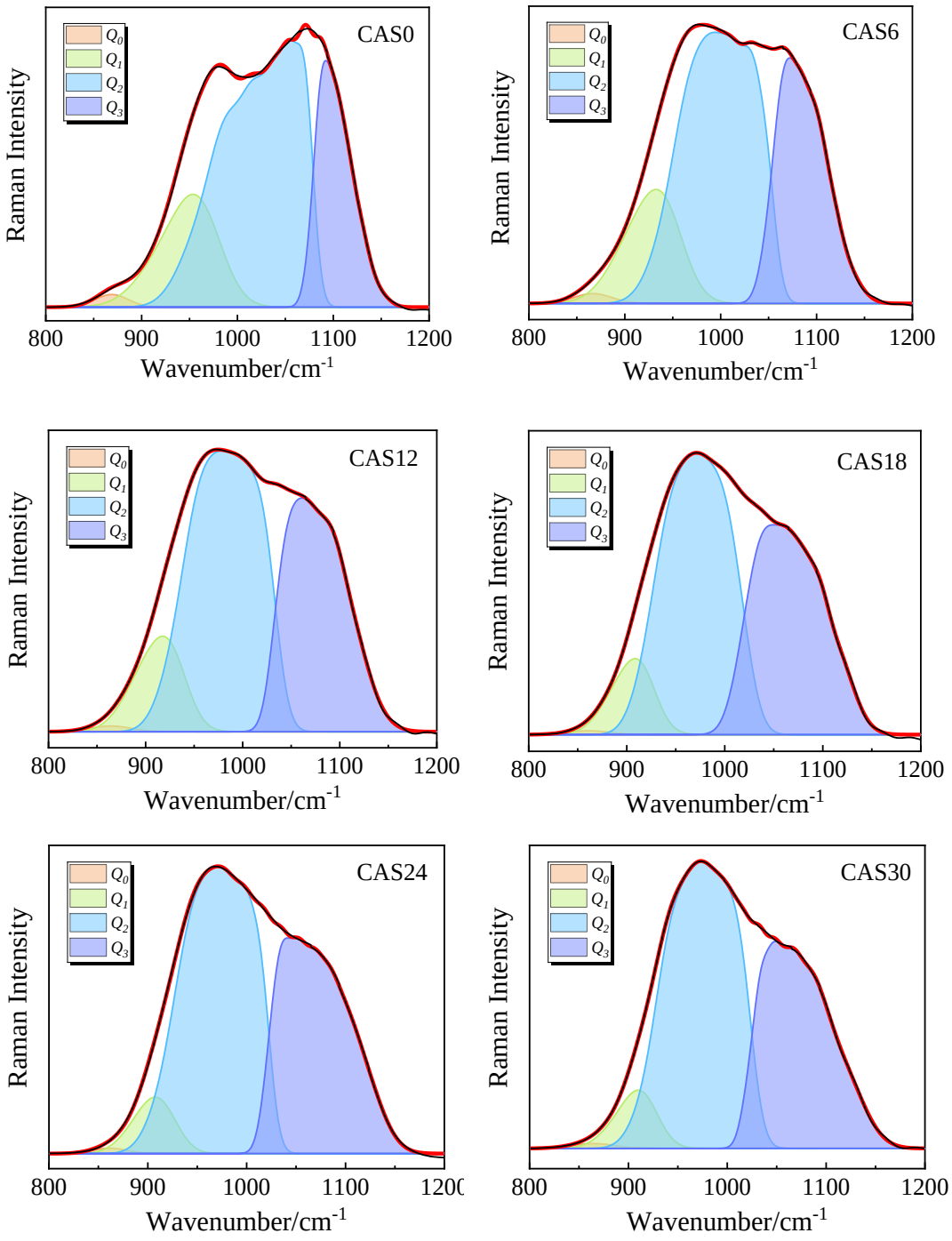

Fig. 11. Four primary structures Q_i (i=0, 1, 2, 3) distributions of Raman spectra of six glassy samples in calcium aluminosilicate, obtained by summing up all the area of delicate $Q^{jklm}_{i\,(n_1h,\,n_2q,\,n_3t)}$ species with the same BO number i.

Additionally, what is noteworthy that Q_4 species cannot be discerned in the range of 800-1200 cm^{-1} of Raman spectrum owing to its absence of Si-O_{nb} bond. Therefore, the abundance of Q_i needs to be calculated separately, and according to the mass balance of the total abundance of NBO and BO, the abundance of Q_i species related to SiOTs should satisfy the following stoichiometric correlations,

$$NBO/Si = \sum_{i=0}^{4}(4-i)X_{Q_i} \quad (4)$$

$$BO/Si = \sum_{i=0}^{4} iX_{Q_i} \quad (5)$$

$$\sum_{i=0}^{4} X_{Q_i} = 1 \quad (6)$$

Where NBO/Si and BO/Si denote the average numbers of NBO and BO per SiOT respectively. X_{Q_i} is the molar fraction of Q_i species. On the other hand, NBO/Si values can be also obtained from the expression [26] ,

$$NBO/Si = \sum_{i=1}^{i} nM_i^{n+}/Si \quad (7)$$

M^{n+} represents network modifying cation, and the sum is obtained after subtraction of the amount of metal cations proportion necessary for charge-balance of AlOTs. In this paper, the content of Al^{IV} has approximately determined by ^{27}Al MAS NMR, the modified correlation, therefore, is given,

$$NBO/Si = \frac{2[n(CaO)-n(Al_2O_3)\cdot X(Al^{IV})]}{n(SiO_2)} \quad (8)$$

$$BO/Si = 4 - \mathrm{NBO/Si} \quad (9)$$

Where X ($Al^{\square}$) is the molar fraction of Al^{IV}. After determining NBO/Si and BO/Si values of glassy samples by Eqs. (8)-(9), Q_4 species contents can be calculated through Eqs. (4)-(6). Fig. 12 shows the quantitative distribution of primary structures Q_i (i=0, 1, 2, 3, 4) as a function of Al_2O_3 concentrations. We can see that various Q_i species coexisting while Q_2 maintains predominant and only a small amount of Q_0 (≤ 1%) was observed in all CAS glassy samples. In addition, a regular trend is captured that Q_3, Q_4 increases and Q_1, Q_2 decrease with adding of alumina from 0 to 18 at CaO/SiO_2 ratios of 1. Whereas, further addition of alumina, continuous reduction is detected on Q_1 and Q_2, while Q_4 increases rapidly, and in contrast to the above, Q_3 shows a decreasing trend while x≥18.

In addition, the values of the average numbers of NBO per SiOT and AlOT (NBO/T) which frequently represents the degree of depolymerization of aluminosilicate network are obtained using Eq. (10).

$$NBO/T = \frac{n(SiO_2)\cdot\sum_{i=0}^{4}(4-i)\cdot X_{Q_i}}{n(SiO_2)+2n(Al_2O_3)\cdot X(Al^{IV})} \quad (10)$$

Fig. 13 presents the degree of polymerization and depolymerization as a function of Al_2O_3 contents. From this figure we can see intuitively that the connectivity of

silicate network increases with adding of Al_2O_3. This can be attributed to the replacement of SiOTs by AlOTs and Ca^{2+} cations are consumed for charge compensators rather than network modifiers, in which induces the transformation of NBOs to BOs.

The 'Loewenstein Al avoidance' rule points out that [36], the connections of Si-O_b-Al^{IV} are energetically more favorable in aluminosilicate, rather than the connections of Al^{IV}-O_b-Al^{IV} which will lead to the accumulation of local negative charges in the structure. Whereas, it has been proved that violation of the rule is possible, especially in alkaline-earth aluminosilicate glasses [62-64]. When the number of Al-O_b linkages is larger than the available Si-O_b linkages, the role of "aluminum-avoidance" is bound to be invalid or different structures will occur, such as Al^{IV}-O_b-Al^{IV} linkages. Based on this, a new parameter called the aluminum-avoidance parameter (AAP) is derived by Amarnath R. Allu *et al.* [62] purposefully to predict the applicability of the role of "aluminum-avoidance", given by Eq. (11).

$$AAP = \frac{4[Al_2O_3]}{2[SiO_2]-[RO]+[Al_2O_3]} \quad (11)$$

The detailed calculation process is referred to [62], which bases on the ratio of the number of Al-O_b and Si-O_b bonds. When AAP＜1, there are sufficient Si-O_b bonds to satisfy the role of "aluminum-avoidance", which will invalid at AAP≥1. For the glassy samples in this study, the AAP values of CAS0 to CAS30 were obtained, are 0, 0.45, 0.86, 1.22, 1.55 and 1.85 respectively, i.e., there is no remaining Si-O_b-Si linkage can be used to break and form Si-O_b-Al^{IV} linkage when x≥18, inducing the production of Al^{IV}-O_b-Al^{IV} linkages or higher coordinated aluminum, which the latter can be confirmed by ^{27}Al MAS NMR results in Fig. 6. There is no experimental evidence to detected the existence of Al^{IV}-O_b-Al^{IV} linkages in x≥18, whereas, it can be indirectly proved, based on the phenomenon of delicate $Q^{jklm}_{i\ (n_1h,\ n_2q,\ n_3t)}$ species do not continue to red shift with the increase of Al_2O_3 content in x≥18 as shown in Fig. 10 that Si-O_b-Al^{IV} linkage would not increase when x≥18. Moreover, what unambiguous is merely inconspicuous abundance of Al^{V} and Al^{VI} species in all glassy samples. Inasmuch as there is still enough Ca^{2+} for charge compensation, it can extrapolate naturally that the excess aluminum has the preference to form Al^{IV}-O_b-Al^{IV} linkages in AAP≥1.

On the variation process of Q_i species, Q_1, Q_2 decrease linearly with increasing Al_2O_3 content, while Q_4 shows a nonlinear increasing firstly before x＜18 (AAP＜1), and then increase linearly. Moreover, Q_3 increases in a nonmonotonic way with Al_2O_3 up to 18% (and AAP is greater than 1), then start decreasing. It is readily to conclude that Q_3 species preferentially be produced with the addition of Al_2O_3 until AAP=1, and with the alumina content exceeds to 18 mol%, fully polymerized Q_4 species increase sharply along with the formation of Al^{IV}-O_b-Al^{IV} bonds. Eventually, the evolution of Q_i leads to the monotonic increase of the degree of polymerization (as shown in Fig. 13).

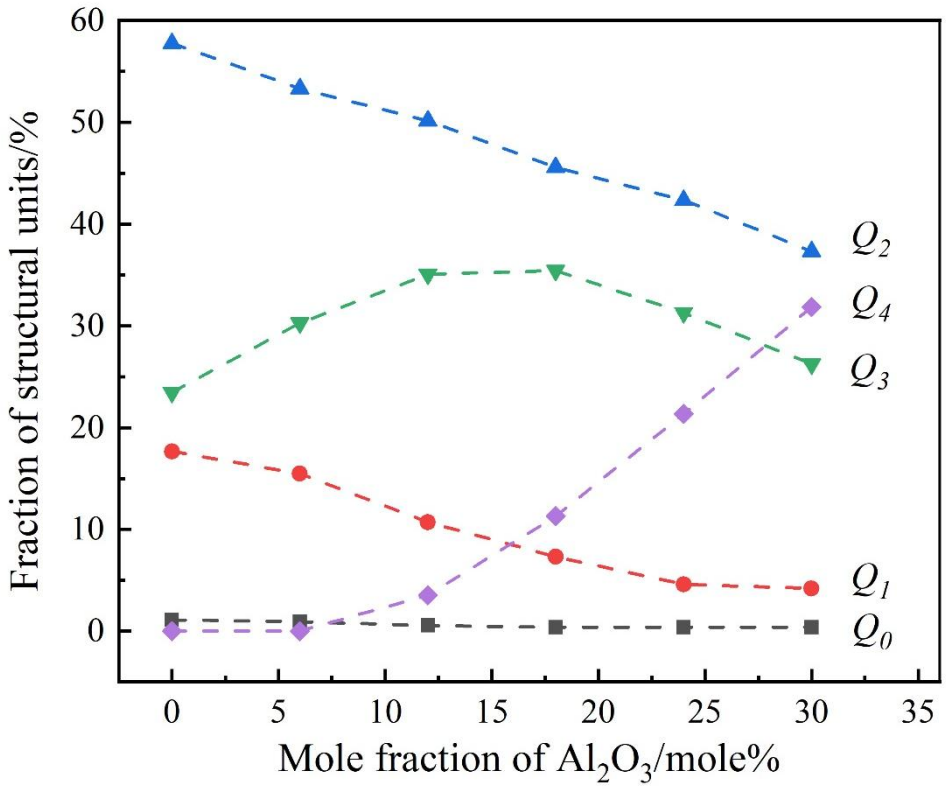

Fig. 12. The quantitative distribution of Q_i (i=0, 1, 2, 3, 4) species of SiOTs with the increase of Al_2O_3 content at a fixed CaO/SiO_2 ratio of 1, determined by Raman spectroscopy in calcium aluminosilicate glasses.

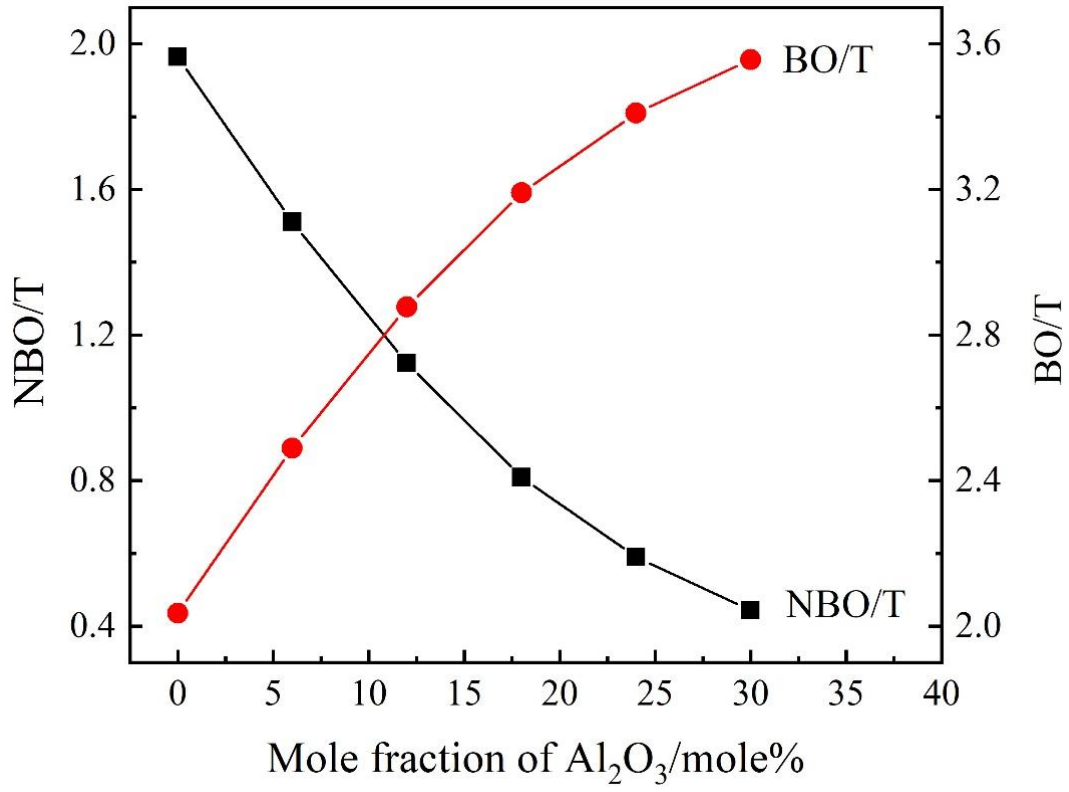

Fig. 13. The variations of NBO/T and BO/T as a function of Al_2O_3 contents.

4. Conclusions

The ever-finer quantitative procedure of Raman spectroscopy was achieved successfully, combined with ^{27}Al MAS NMR and QC *ab initio* calculations, to investigate the microstructural characteristics of calcium aluminosilicate glasses with various Al_2O_3 contents and at a fixed CaO/SiO_2 ratio of 1. The relationship between *RSCS* and *SIT* was established to correct the experimental Raman spectra. The fitting results of ^{27}Al MAS NMR showed that, since $CaO/Al_2O_3>1$ was always satisfied, aluminum atoms primarily existed in four-fold coordinated Al^{IV} sites while around 5% five-fold coordinated Al^{V} and minute six-fold coordinated Al^{VI} were detected, simultaneously.

The quantitative description with Q_i species by Raman spectroscopy was performed, which showed a significant adjustment of Q_i species distribution of aluminosilicate glasses with the addition of Al_2O_3. In detail, Q_1 and Q_2 decrease linearly with increasing Al_2O_3 content, while Q_3 preferentially produces at $x<18$ ($AAP<1$) and decreases further adding Al_2O_3, meanwhile fully polymerized Q_4 increases dramatically, notably when $x\geqslant18$ ($AAP>1$). It can be attributed to the producing of AlOTs as network formers through consuming Ca^{2+} cations as charge compensators before as network modifiers, results in the continuous increase of the degree of polymerization. In the other hand, the appearance of Al^{IV}-O_b-Al^{IV} bonds was proved by hyperfine deconvolution results of Raman spectroscopy and ^{27}Al MAS NMR at $x\geqslant18$ ($AAP>1$). These knowledges will provide very valuable basis for further studies of melt microstructure and corresponding physical and chemical properties of calcium aluminosilicate.

Acknowledgements

This work was supported by National Natural Science Foundation of China (21773152, 22003039), National 111 project (D17002, the Program of Introducing Talents of Discipline to Universities), the Key Basic Research Projects of the Basic Strengthening Plan of the Commission of Science and Technology(2021-JCJQ-ZD-051-00-02), the Shanghai Committee of Science and Technology Fund, China (12520709200), the Open Project Program of the State Key Laboratory of Advanced Special Steel, Shanghai University, China (SKLASS2020-06) and Special Fund Project of Shanghai Municipality for Science and Technology Development (YDZX20173100001316), the China Scholarship Council under the Grant CSC No. 202006890136.

References

[1] L. Sharma, R. Chhibber, Design & development of SAW fluxes using $CaO–SiO_2–CaF_2$ and $CaO–SiO_2–Al_2O_3$ flux systems, Ceramics International, 46 (2020) 1419-1432.

[2] V.E. Sokol'skii, D. Pruttskov, V. Busko, V. Kazimirov, O. Roik, A. Chyrkin, V. Galinich, I. Goncharov, Investigation of structure of $CaO-Al_2O_3-SiO_2$ melts as a basis for the development of new agglomerated welding fluxes and industrial refractories, Journal of Mining and Metallurgy, Section B: Metallurgy, 54 (2018) 133-141.

[3] J.L. Li, Q.F. Shu, K. Chou, Effect of Al_2O_3/SiO_2 mass ratio on viscosity of $CaO–Al_2O_3–SiO_2–CaF_2$ slag, Ironmaking & Steelmaking, 42 (2014) 154-160.

[4] S. Takahashi, D.R. Neuville, H. Takebe, Thermal properties, density and structure of percalcic and peraluminus $CaO–Al_2O_3–SiO_2$ glasses, Journal of Non-Crystalline Solids, 411 (2015) 5-12.

[5] N. Sano, W.-K. Lu, P.V. Riboud, M. Maeda, Advanced physical chemistry for process metallurgy, Academic Press1997.

[6] J.L. You, G.C. Jiang, H.Y. Hou, H. Chen, Y.Q. Wu, K.D. Xu, Quantum chemistry study on superstructure and Raman spectra of binary sodium silicates, Journal of Raman Spectroscopy: An International Journal for Original Work in all Aspects of Raman Spectroscopy, Including Higher Order Processes, and also Brillouin and Rayleigh Scattering, 36 (2005) 237-249.

[7] Y.-L. Zhen, G.-H. Zhang, X.-L. Tang, K.-C. Chou, Influences of Al_2O_3/CaO and Na_2O/CaO ratios on viscosities of $CaO-Al_2O_3-SiO_2-Na_2O$ melts, Metallurgical and Materials Transactions B, 45 (2014) 123-130.

[8] M. Edén, Update on ^{27}Al NMR studies of aluminosilicate glasses, Annual Reports on NMR Spectroscopy, Elsevier2020, pp. 285-410.

[9] D.R. Neuville, L. Cormier, D. Massiot, Al coordination and speciation in calcium aluminosilicate glasses: Effects of composition determined by ^{27}Al MQ-MAS NMR and Raman spectroscopy, Chemical geology, 229 (2006) 173-185.

[10] S.K. Lee, J.F. Stebbins, Disorder and the extent of polymerization in calcium silicate and aluminosilicate glasses: O-17 NMR results and quantum chemical molecular orbital calculations, Geochimica et Cosmochimica Acta, 70 (2006) 4275-4286.

[11] W.J. Malfait, R. Verel, P. Ardia, C. Sanchez-Valle, Aluminum coordination in rhyolite and andesite glasses and melts: Effect of temperature, pressure, composition and water content, Geochimica et Cosmochimica Acta, 77 (2012) 11-26.

[12] D. Neuville, L. Cormier, D. De Ligny, J. Roux, A. Flank, P. Lagarde, Environments around Al, Si, and Ca in aluminate and aluminosilicate melts by X-ray absorption spectroscopy at high temperature, American Mineralogist, 93 (2008) 228-234.

[13] K. Kanehashi, J.F. Stebbins, In situ high temperature ^{27}Al NMR study of structure and dynamics in a calcium aluminosilicate glass and melt, Journal of Non-Crystalline Solids, 353 (2007) 4001-4010.
[14] J.L. Yarger, K. Smith, R.A. Nieman, J. Diefenbacher, G.H. Wolf, B.T. Poe, P.F. McMillan, Al coordination changes in high-pressure aluminosilicate liquids, Science, 270 (1995) 1964-1967.
[15] W. Yan, G. Zhang, J. Li, Viscosity and structure evolution of $CaO–SiO_2$-based mold fluxes with involvement of $CaO–Al_2O_3$-based tundish fluxes, Ceramics International, 46 (2020) 14078-14089.
[16] Z. Wang, G. Wen, Q. Liu, S. Huang, P. Tang, L. Yu, Estimating the thermal conductivity of $CaO–Al_2O_3–SiO_2$ slags by equilibrium molecular dynamics simulations, Journal of Non-Crystalline Solids, 531 (2020) 119851.
[17] Z.-G. Yu, H.-Y. Leng, L.-J. Wang, K.-C. Chou, Computational study on various properties of $CaO-Al_2O_3-SiO_2$ mold flux, Ceramics International, 45 (2019) 7180-7187.
[18] R. Rajavaram, H. Kim, J. Park, C.-H. Lee, W.-S. Cho, J. Lee, Bridging between the physical properties: structure and density of $CaO-SiO_2-Al_2O_3$ melts at CaO/SiO_2= 1.3 and different mole% of Al_2O_3, Ceramics International, 45 (2019) 19409-19414.
[19] R. Rajavaram, H. Kim, C.-H. Lee, W.-S. Cho, C.-H. Lee, J. Lee, Effect of Al_2O_3 Concentration on Density and Structure of $(CaO-SiO_2)-xAl_2O_3$ Slag, Metallurgical and Materials Transactions B, 48 (2017) 1595-1601.
[20] H. Doweidar, Density of $CaO–Al_2O_3–SiO_2$ glasses with $(CaO/Al_2O_3)\geq 1$; the hidden factors, Journal of Non-Crystalline Solids, 471 (2017) 344-348.
[21] Z. Wang, I. Sohn, Effect of the Al_2O_3/SiO_2 mass ratio on the crystallization behavior of $CaO-SiO_2-MgO-Al_2O_3$ slags using confocal laser scanning microscopy, Ceramics International, 44 (2018) 19268-19277.
[22] Y. Kang, K. Morita, Thermal conductivity of the $CaO–Al_2O_3–SiO_2$ system, ISIJ international, 46 (2006) 420-426.
[23] B.O. Mysen, A. Lucier, G.D. Cody, The structural behavior of Al^{3+} in peralkaline melts and glasses in the system $Na_2O-Al_2O_3-SiO_2$, American Mineralogist, 88 (2003) 1668-1678.
[24] J. You, G. Jiang, K. Xu, High temperature Raman spectra of sodium disilicate crystal, glass and its liquid, Journal of non-crystalline solids, 282 (2001) 125-131.
[25] B.O. Mysen, Effect of pressure, temperature, and bulk composition on the structure and species distribution in depolymerized alkali aluminosilicate melts and quenched melts, Journal of Geophysical Research: Solid Earth, 95 (1990) 15733-15744.
[26] B.O. Mysen, D. Virgo, F.A. Seifert, Relationships between properties and structure of aluminosilicate melts, American Mineralogist, 70 (1985) 88-105.
[27] J. Ma, M. Wang, J. You, K. Tang, L. Lu, S. Wan, J. Wang, X. Gong, Y. Wang, Quantitative studies on the structure of $xCaO\cdot(1-x)\ SiO_2$ glasses and melts by in-situ Raman spectroscopy, ^{29}Si MAS NMR and quantum chemistry ab initio calculation, Journal of Non-Crystalline Solids, 546 (2020) 120252.

[28] M. Wang, P. Simon, L. Lu, A.A. Sobol, J. Wang, S. Wan, J. You, Quantitative studies on the structure of molten binary potassium molybdates by in situ Raman spectroscopy and quantum chemistry ab initio calculations, Analytical chemistry, 90 (2018) 9085-9092.
[29] J.H. Park, Structure–property relationship of CaO-MgO-SiO_2 slag: quantitative analysis of Raman spectra, Metallurgical and Materials Transactions B, 44 (2013) 938-947.
[30] J.H. Park, Structure–property correlations of CaO–SiO_2–MnO slag derived from Raman spectroscopy, ISIJ international, 52 (2012) 1627-1636.
[31] Y. Jinglin, G. Jiang, C. Hui, X. Kuangdi, Raman spectra and structure study of silicate glasses and their liquids, Rare Metals, 25 (2006) 431-436.
[32] N. Umesaki, M. Takahashi, M. Tatsumisago, T. Minami, Structure of rapidly quenched glasses in the system Li_2O-SiO_2, Journal of materials science, 28 (1993) 3473-3481.
[33] X. Gong, J. Wang, J. You, M. Wang, X. Tang, F. Zhang, K. Tang, L. Lu, S. Wan, Q. Zhang, Room temperature Raman spectroscopy and ^{29}Si MAS NMR combined with high temperature Raman spectroscopy and DFT calculation of xMgO-(1-x) CaO–SiO_2 glasses and melts, Ceramics International, 48 (2022) 4911-4920.
[34] M. Nowak, H. Rostkowska, L. Lapinski, J. Kwiatkowski, J. Leszczynski, Experimental matrix isolation and theoretical ab initio HF/6-31G (d, p) studies of infrared spectra of purine, adenine and 2-chloroadenine, Spectrochimica Acta Part A: Molecular Spectroscopy, 50 (1994) 1081-1094.
[35] T.J. Lee, D. Jayatilaka, An open-shell restricted Hartree—Fock perturbation theory based on symmetric spin orbitals, Chemical physics letters, 201 (1993) 1-10.
[36] W. Loewenstein, The distribution of aluminum in the tetrahedra of silicates and aluminates, American Mineralogist: Journal of Earth and Planetary Materials, 39 (1954) 92-96.
[37] B. Piriou, P. McMillan, The high-frequency vibrational spectra of vitreous and crystalline orthosilicates, American Mineralogist, 68 (1983) 426-443.
[38] S.A. Brawer, W.B. White, Raman spectroscopic investigation of the structure of silicate glasses (II). Soda-alkaline earth-alumina ternary and quaternary glasses, Journal of Non-Crystalline Solids, 23 (1977) 261-278.
[39] G. Greaves, S. Sen, Inorganic glasses, glass-forming liquids and amorphizing solids, Advances in physics, 56 (2007) 1-166.
[40] I. Avramov, C. Rüssel, R. Keding, Effect of chemical composition on viscosity of oxide glasses, Journal of non-crystalline solids, 324 (2003) 29-35.
[41] W.-A. Buckermann, W. Müller-Warmuth, G. Heinz Frischat, A further ^{29}Si MAS NMR study on binary alkali silicate glasses, Glastechnische Berichte, 65 (1992) 18-21.
[42] J.F. Stebbins, Effects of temperature and composition on silicate glass structure and dynamics: Si-29 NMR results, Journal of Non-Crystalline Solids, 106 (1988) 359-369.
[43] B. Mysen, P. Richet, Developments in geochemistry, Silicate glasses and melts: properties and structure, Elsevier New York2005.

[44] B. Mysen, Aluminosilicate melts: structure, composition and temperature, Contributions to Mineralogy and Petrology, 127 (1997) 104-118.
[45] H. Maekawa, T. Maekawa, K. Kawamura, T. Yokokawa, The structural groups of alkali silicate glasses determined from ^{29}Si MAS-NMR, Journal of Non-Crystalline Solids, 127 (1991) 53-64.
[46] P. Feng, Y. Xuehui, M. Xuanxue, Y. Jinglin, W. Chen, C. Hui, J. Guochang, Raman Active Vibrations of Aluminosilicates, Spectroscopy and Spectral Analysis, 26 (2006) 1871-1875.
[47] X. Jun, A Raman spectroscopy study of hyperfine structure of aluminosilicate and feldspar, China University of Geosciences (Beijing), 2008.
[48] K.J. MacKenzie, M.E. Smith, Multinuclear solid-state nuclear magnetic resonance of inorganic materials, Elsevier2002.
[49] J.F. Stebbins, S. Kroeker, S.K. Lee, T. Kiczenski, Quantification of five-and six-coordinated aluminum ions in aluminosilicate and fluoride-containing glasses by high-field, high-resolution ^{27}Al NMR, Journal of Non-Crystalline Solids, 275 (2000) 1-6.
[50] S. Sukenaga, T. Nagahisa, K. Kanehashi, N. Saito, K. Nakashima, Reconsideration on Al coordination in $CaO–SiO_2–Al_2O_3–(R_2O$ or $RO)$ glasses by using high field solid-state ^{27}Al NMR spectroscopy, ISIJ international, 51 (2011) 333-335.
[51] D. Massiot, F. Fayon, M. Capron, I. King, S. Le Calvé, B. Alonso, J.-O. Durand, B. Bujoli, Z. Gan, G. Hoatson, Modelling one- and two-dimensional solid-state NMR spectra, Magnetic Resonance in Chemistry, 40 (2002) 70-76.
[52] D. Neuville, L. Cormier, V. Montouillout, D. Massiot, Local Al site distribution in aluminosilicate glasses by ^{27}Al MQMAS NMR, Journal of Non-Crystalline Solids, 353 (2007) 180-184.
[53] D.R. Neuville, L. Cormier, D. Massiot, Al environment in tectosilicate and peraluminous glasses: A ^{27}Al MQ-MAS NMR, Raman, and XANES investigation, Geochimica et Cosmochimica Acta, 68 (2004) 5071-5079.
[54] J.R. Allwardt, S.K. Lee, J.F. Stebbins, Bonding preferences of non-bridging O atoms: Evidence from ^{17}O MAS and 3QMAS NMR on calcium aluminate and low-silica Ca-aluminosilicate glasses, American Mineralogist, 88 (2003) 949-954.
[55] B. Hehlen, D.R. Neuville, Raman response of network modifier cations in alumino-silicate glasses, J Phys Chem B, 119 (2015) 4093-4098.
[56] B. Mysen, D. Virgo, Structure and Properties of Silicate Glasses and Melts; Theories and Experiment, Advanced Mineralogy, Springer1994, pp. 238-254.
[57] M.J. Pelletier, Quantitative analysis using Raman spectrometry, Applied spectroscopy, 57 (2003) 20A-42A.
[58] S. Fábio, A. Adailton, B. Mauricelio, B. Karla, B. Jean-Louis, C. Ewerton, M. Roberto, F. Valder, R. Ariete, P. Raman, FTIR, and DFT study of $Na_2Ti_3O_7$ microcrystals, J RAMAN SPECTROSC, 49 (2018) 538-548.
[59] K. Łuczyńska-Szymczak, W. Starosta, K. Drużbicki, Solid-state DFT-assisted Raman study of titaniate nanostructures, Spectrochimica Acta Part A: Molecular and Biomolecular Spectroscopy, 116 (2013) 646-650.

[60] P. Zhang, P.J. Grandinetti, J.F. Stebbins, Anionic species determination in $CaSiO_3$ glass using two-dimensional ^{29}Si NMR, The Journal of Physical Chemistry B, 101 (1997) 4004-4008.
[61] P. Zhang, C. Dunlap, P. Florian, P. Grandinetti, I. Farnan, J. Stebbins, Silicon site distributions in an alkali silicate glass derived by two-dimensional ^{29}Si nuclear magnetic resonance, Journal of Non-Crystalline Solids, 204 (1996) 294-300.
[62] A.R. Allu, A. Gaddam, S. Ganisetti, S. Balaji, R.e. Siegel, G.C. Mather, M. Fabian, M.J. Pascual, N. Ditaranto, W. Milius, Structure and crystallization of alkaline-earth aluminosilicate glasses: prevention of the alumina-avoidance principle, The Journal of Physical Chemistry B, 122 (2018) 4737-4747.
[63] S.K. Lee, H.-I. Kim, E.J. Kim, K.Y. Mun, S. Ryu, Extent of disorder in magnesium aluminosilicate glasses: Insights from ^{27}Al and ^{17}O NMR, The Journal of Physical Chemistry C, 120 (2016) 737-749.
[64] S.K. Lee, J.F. Stebbins, The degree of aluminum avoidance in aluminosilicate glasses, American Mineralogist, 84 (1999) 937-945.